22. A. Crida, A. Morbidelli, F. Masset, *Icarus* **181**, 587 (2006).
23. S. E. Dodson-Robinson, C. Salyk, *Astrophys. J.* **738**, 131 (2011).
24. Z. Zhu, R. P. Nelson, R. Dong, C. Espaillat, L. Hartmann, *Astrophys. J.* **755**, 6 (2012).
25. S. M. Andrews, J. P. Williams, *Astrophys. J.* **631**, 1134 (2005).
26. J.-W. Xie, M. J. Payne, P. Thébault, J.-L. Zhou, J. Ge, *Astrophys. J.* **724**, 1153 (2010).
27. F. Windmark *et al.*, *Astron. Astrophys.* **540**, A73 (2012).
28. D. C. Jewitt, J. X. Luu, in *Protostars and Planets IV*, V. Mannings, S. S. Russell, A. Boss, Eds. (Univ. of Arizona Press, Tucson, AZ, 2000), p. 1201.
29. C. Marois *et al.*, *Science* **322**, 1348 (2008).
30. A.-M. Lagrange *et al.*, *Science* **329**, 57 (2010).

Acknowledgments: We thank M. Benisty and W. Lyra for useful discussions. This paper makes use of the following ALMA data: ADS/JAO.ALMA no. 2011.0.00635.SSB. ALMA is a partnership of the European Southern Observatory (ESO) (representing its member states), NSF (USA), and National Institutes of Natural Sciences (Japan), together with the National Research Council (Canada) and National Science Council and Academia Sinica Institute of Astronomy and Astrophysics (Taiwan), in cooperation with the Republic of Chile. The Joint ALMA Observatory is operated by the ESO, Associated Universities Inc./National Radio Astronomy Observatory, and National Astronomical Observatory of Japan. The data presented here are archived at www.alma-allegro.nl/science, and the full project data (2011.0.00635.SSB) will be publicly available at the ALMA Science Data Archive, https://almascience.nrao.edu/alma-data/archive.

Supplementary Materials

www.sciencemag.org/cgi/content/full/340/6137/1199/DC1
Materials and Methods
Figs. S1 to S5
References (*31*–*54*)

19 February 2013; accepted 7 May 2013
10.1126/science.1236770

Coupling a Single Trapped Atom to a Nanoscale Optical Cavity

J. D. Thompson,[1]* T. G. Tiecke,[1,2]* N. P. de Leon,[1,3] J. Feist,[1,4] A. V. Akimov,[1,5] M. Gullans,[1] A. S. Zibrov,[1] V. Vuletić,[2] M. D. Lukin[1]†

Hybrid quantum devices, in which dissimilar quantum systems are combined in order to attain qualities not available with either system alone, may enable far-reaching control in quantum measurement, sensing, and information processing. A paradigmatic example is trapped ultracold atoms, which offer excellent quantum coherent properties, coupled to nanoscale solid-state systems, which allow for strong interactions. We demonstrate a deterministic interface between a single trapped rubidium atom and a nanoscale photonic crystal cavity. Precise control over the atom's position allows us to probe the cavity near-field with a resolution below the diffraction limit and to observe large atom-photon coupling. This approach may enable the realization of integrated, strongly coupled quantum nano-optical circuits.

Trapped, ultracold atoms coupled to nanoscale optical cavities are exemplary hybrid quantum systems (*1*, *2*), with potential applications ranging from single-photon nonlinear optics (*3*–*7*) to quantum networks (*8*, *9*). However, realizing the largest interaction strengths requires placing and controlling an atom very close to a surface, within the near field of the confined optical mode, as set by the reduced atomic resonance wavelength of $\lambda/(2\pi) \sim 125$ nm for rubidium (Rb). Position control at this level has been achieved for single atoms in free space and in micrometer-scale cavities by using standing waves (*10*, *11*) or high numerical-aperture optics (*12*, *13*). Achieving similar control close to surfaces is much more challenging because attractive atom-surface forces are comparable with typical trapping forces for cold atoms in this regime. Previously, atomic ensembles have been stably trapped at distances of 500 nm from a surface by using magnetic traps formed by patterned electrodes (*14*, *15*) and down to 215 nm by using optical dipole traps based on evanescent waves (*16*, *17*).

Our technique to position an atom near an arbitrary nanoscale object uses a tightly focused optical tweezer beam (*18*) that is retro-reflected from the nanoscale object itself (*19*, *20*) and red-detuned from the atomic resonance (Fig. 1A).

[1]Department of Physics, Harvard University, Cambridge, MA 02138, USA. [2]Department of Physics, Massachusetts Institute of Technology (MIT)–Harvard Center for Ultracold Atoms, and Research Laboratory of Electronics, MIT, Cambridge, MA 02139, USA. [3]Department of Chemistry and Chemical Biology, Harvard University, Cambridge, MA 02138, USA. [4]Institute for Theoretical Atomic Molecular and Optical Physics (ITAMP), Harvard-Smithsonian Center for Astrophysics, Cambridge, MA 02138, USA. [5]Russian Quantum Center, Skolkovo, Moscow Region 143025, Russia.

*These authors contributed equally to this work.
†Corresponding author. E-mail: lukin@physics.harvard.edu

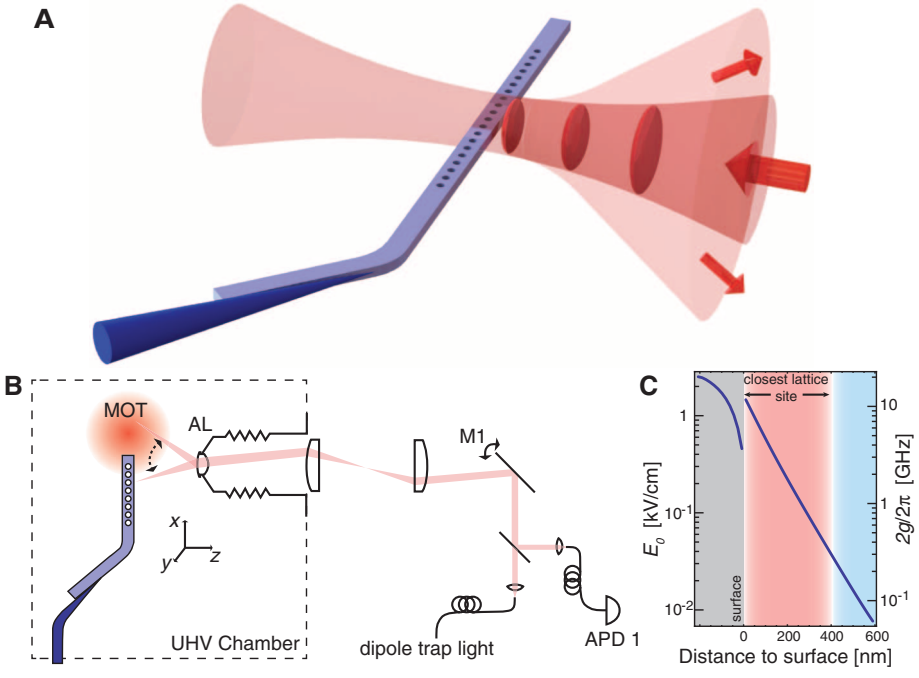

Fig. 1. Experimental concept. (**A**) The atom trap near a nanoscale solid-state structure (here, a photonic crystal waveguide) arises from the interference of an optical tweezer with its reflection from the structure, which forms a standing-wave optical lattice. (**B**) A single atom is loaded from a free-space MOT into a dipole trap formed by an aspheric lens (AL) and steered by a galvanometer mirror (M1). Fluorescence on APD1 signals the presence of an atom and triggers the motion of the dipole trap to the nanostructure. UHV, ultrahigh vacuum. (**C**) The single-photon electric field strength E_0 and single-photon Rabi frequency $2g = 2E_0/\hbar$ at a given distance from the outer surface of a PWC cavity, using $\lambda_T = 815$ nm (d is the atomic dipole moment and $\hbar$ is Planck's constant h divided by 2π). The range of distances that can be chosen for the closest lattice site is indicated. As discussed in the text, surface forces and currently realized trap depths limit the achievable distance to $z_0 \approx 100$ nm, at which point $2g/(2\pi)$ is several GHz.

The resulting standing-wave optical lattice has a local intensity maximum, corresponding to a minimum of the potential energy, at a typical distance $z_0 \sim \lambda_T/4$ from the surface, with additional maxima farther away spaced in increments of $\lambda_T/2$ (λ_T is the trap laser wavelength). The lateral position of the trap can be controlled by moving the focused incident beam, whereas the distance z_0 depends on the phase shift of the reflected light, which is determined by the geometry of the nanostructure. In certain cases, changing the structure dimensions allows z_0 to be tuned between nearly 0 and $\lambda_T/2$ (figs. S3 and S4). Crucially, the lattice site closest to the surface can be loaded with a single atom from a conventional free-space optical tweezer simply by scanning the latter onto and over the surface, provided the atom has been originally prepared at sufficiently low temperature (*21*). Even though the attractive van der Waals interaction between the atom and the surface limits the minimum trap distance to about 100 nm for realistic laser intensities (*22*), this method nevertheless allows for direct, strong, and reproducible near-field optical coupling of atoms to solid-state nanostructures of interest.

The nanostructure in the present experiment is a photonic crystal waveguide cavity (PWC) that is mounted to a tapered optical fiber tip and placed in the focal plane of a high numerical aperture lens (Fig. 1, A and B, and fig. S1). A magneto-optical trap (MOT) was formed near the fiber tip and used to load the optical tweezer (λ_T = 815 nm, beam waist w = 900 nm, and potential depth U_0/k_B = 1.6 mK, where k_B is the Boltzmann constant) with one atom at a distance of 40 μm from the nanostructure. [The presence of only a single atom is ensured by the collisional blockade effect (*18*).] After a period of Raman sideband cooling to the vibrational ground state in the two radial directions, and to a few vibrational quanta in the direction along the tweezer (*21*), we translated the optical tweezer using a scanning galvanometer mirror (Fig. 1B) until it was aimed directly at the nanostructure, loading the atom into the lattice.

We first verified that we can load the lattice site closest to the surface by positioning an atom near a bare tapered nanofiber tip (Fig. 2, A and B) without the PWC present. We distinguished the lattice sites spectroscopically by means of a weak, off-resonant probe beam guided by the nanofiber. This beam produces a substantial differential AC Stark shift between the ground-state hyperfine levels for an atom in lattice site A, and a much smaller shift for atoms in more distant lattice sites (*22*). The microwave-frequency spectra on the $|F = 1, m_F = 0\rangle \leftrightarrow |2,0\rangle$ transition is shown in Fig. 2C, obtained by focusing the tweezer in different z planes before loading the lattice (F and m_F indicate the atomic hyperfine and magnetic quantum numbers, respectively). Two distinct peaks appear: one near the unperturbed transition frequency at f_B and another shifted by 150 kHz at f_A, which we identify as the Stark-shifted resonance frequency in the lattice site closest to the fiber. This identification was made by measuring the coupling of the atomic fluorescence into the fiber. Assuming lossless propagation in the fiber taper, we expected a collection efficiency in the closest (second closest) lattice site of 4% (0.2%); the measured value in site A is (1.5 ± 0.6)% >> 0.2%. This confirms that site A is the closest site to the fiber. The discrepancy with the expected value is attributed to losses in the fiber taper (*22*). From the data in Fig. 2C, we conclude that 100^{+0}_{-12}% of the atoms that survive the loading procedure are in the closest lattice site. Additional measurements show that 94 ± 6% of all atoms survive the loading process (after subtracting losses due to collisions with the background gas), so we conclude that the first lattice site may be loaded deterministically, with an unconditional fidelity of 94^{+6}_{-13}%.

We next describe coupling an atom to the optical resonance of a PWC (*23*) fabricated in silicon nitride (Fig. 3, A to C). We attached the PWC to a tapered optical fiber tip, which provides both an efficient optical interface to the cavity and mechanical support. Because of the nanoscale dimensions of the waveguide, an appreciable evanescent field resides outside the waveguide, which allows for coupling to an atom trapped in this region without the need to place the atom inside the holes (*24*, *25*). As shown in Fig. 1C, single-photon Rabi frequencies $2g = 2\mathbf{d} \cdot \mathbf{E}/\hbar$ in the range of several gigahertz (corresponding to single-photon electric fields of several hundred volts per centimeter) are accessible for the atom-surface distances that can be realized with the present trapping technique, which is large relative to other cavity quantum electrodynamics (QED) approaches with neutral atoms. For example, $2g/(2\pi)$ = 430 MHz is the current state of the art in Fabry-Perot cavities (*11*), and $2g/(2\pi) \approx$ 200 MHz has been realized with microtoroid optical resonators (*3*).

To demonstrate the coupling of the atom to the cavity mode as well as the sub-wavelength position control of the atom, we mapped out the intensity distribution of the cavity mode by scanning the atom along the waveguide. The local intensity is measured by pumping the cavity weakly with a laser tuned near the $F = 2 \rightarrow F' = 2$ transition of the D2 line and measuring the optical

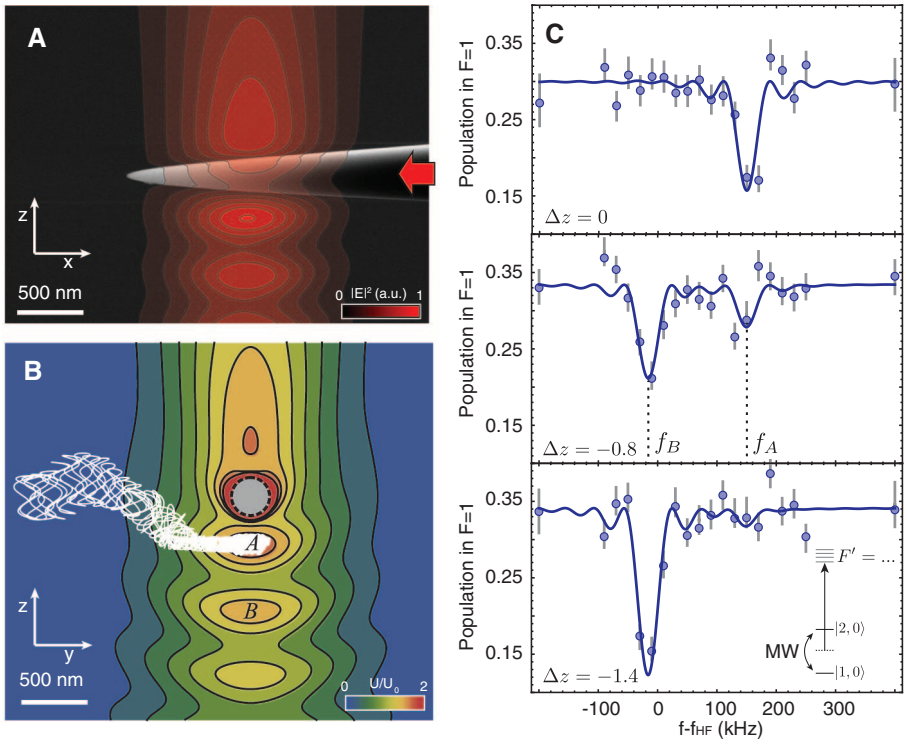

Fig. 2. Loading the optical lattice near the surface. (**A**) A scanning electron microscope (SEM) image of a tapered nanofiber tip, overlaid with the simulated optical tweezer intensity in the *xz* plane [carried out with a finite-difference time-domain (FDTD) method]. (**B**) Numerical simulation of loading process. Color map shows the trapping potential in the *yz* plane [including surface forces (*22*)] with the tweezer pointed directly at the nanofiber. The color scale is normalized to the potential depth of the tweezer in free space, U_0. The white line shows the trajectory of a typical trapped atom with energy E = 3 k_B × 10 μK as the tweezer focus is scanned in the $\hat{y}$ direction. "A" indicates the closest lattice site, and "B" indicates the next closest lattice site. (**C**) Hyperfine transition spectra on the $|1,0\rangle \leftrightarrow |2,0\rangle$ transition, probing the atom-fiber separation. The (f_A,f_B) peaks show atoms loaded into the (A, B, and more distant) lattice sites. The focal plane of the tweezer is displaced by Δz from the fiber midplane in each graph; in this way, different lattice sites can be loaded. At Δz = 0, the absence of a peak at f_B indicates that 100^{+0}_{-12}% of the atoms in the lattice are in the closest site.

pumping rate from $|F = 2, m_F = -2\rangle$ to $F = 1$ (Fig. 3D). The numerically simulated cavity mode is a standing wave (with a period given by the PWC lattice constant, $a \sim 290$ nm), modulated over several micrometers by a Gaussian-like envelope with two lobes. Both features are visible in the data. Because of the tight transverse confinement of the optical field provided by the waveguide, the standing wave is expected to have only 50% contrast: There are no real intensity nodes. The observed contrast is less than than this, so as shown in Fig. 3D, the simulation is convolved with a Gaussian with a root-mean-square (RMS) width of $\delta x_{rms} = 95$ nm. This blurring arises from drift in the tweezer alignment over the course of the measurement (32 hours), jitter in the galvanometer mirror (50 nm RMS), and motion of the atom in the trap. The RMS zero-point atomic motion is 15 to 20 nm, and the thermal motion could be somewhat larger because of heating from technical effects during the experimental sequence. Viewed as a noninvasive probe of the cavity intensity distribution, this technique has a spatial resolution of $2\,\delta x_{RMS} = 190(30)$ nm, following the Sparrow resolution criterion.

Next, we quantified the atom-cavity coupling strength by measuring the reduction of the cavity transmission induced by a single atom. Given the cooperativity $\eta \equiv (2g)^2 / (\kappa\Gamma)$—where κ and Γ are the full linewidths of the cavity and the atomic excited $5P_{3/2}$ state, respectively—the transmission in the presence of an (unsaturated) resonant atom is given by $T = (1 + \eta)^{-2}$ (*5*). To

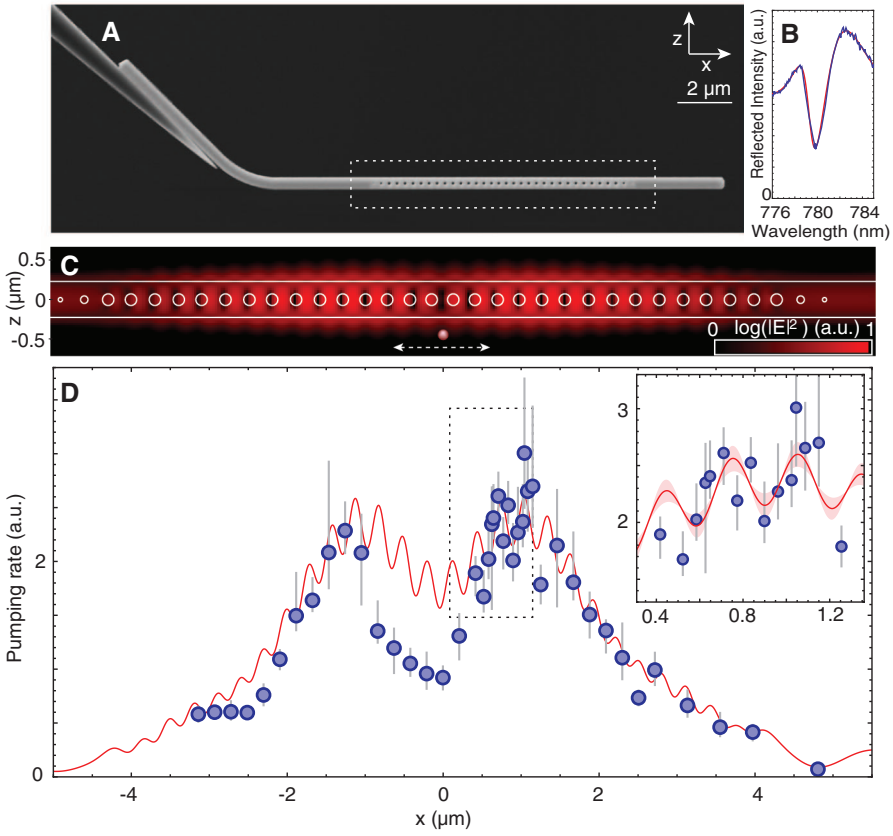

Fig. 3. Coupling a single atom to a photonic crystal cavity. (**A**) An SEM image of a typical PWC attached to a tapered optical fiber. The fiber serves as both a mechanical support and an optical interface to the cavity. (**B**) Reflection spectrum of the PWC resonance near 780 nm, measured through the optical fiber. The line is a fit to a Lorentzian plus a background of Fabry Perot modes of the waveguide, yielding $Q = 460(40)$ and $\lambda_0 = 779.5(1)$ (full spectrum is available in fig. S2). (**C**) Simulation of the PWC resonance at 779.5 nm, overlaid with a cross section of the structure. The simulated mode volume is $V = 0.89\ \lambda^3$. (**D**) Measurement of the intensity distribution of the cavity using a trapped atom. Error bars reflect 1 SD in the fitted pumping rates. The red line shows a model based on simulations of the cavity mode. The systematic disagreement on the left side of the waveguide may be due to interference with background light from the fiber that is not coupled into the waveguide. (Inset) In a set of points acquired in a continuous 8-hour window so as to minimize alignment drift, the standing wave structure of the cavity mode is visible.

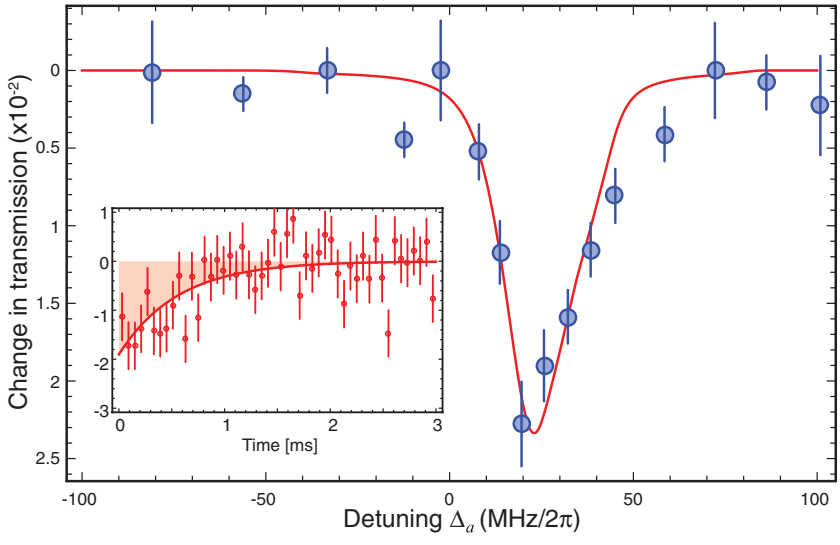

Fig. 4. Change in cavity transmission from a single atom. The transmission of a weak probe beam tuned to the $F = 2 \rightarrow F = 3$ transition is measured versus detuning from the atomic resonance $\Delta_a = \omega_l - \omega_a$, with (ω_l, ω_a) = (laser, zero-field atomic transition) frequency. The cavity resonance remains fixed at $\omega_a + 0.3\ \kappa$. Error bars reflect 1 SD in the fitted transmission reduction. The line is a fit to a numerical model described in the text, yielding $2g = 2\pi \times 600(80)$ MHz. (**Inset**) Transmission versus time for continuous wave probe pulse at $\Delta_a = 27$ MHz. The cavity transmission is initially suppressed; after ~1 ms, the atom is heated by the probe laser and lost from the trap, restoring transmission. Error bars show shot noise in the number of detected photons; the data are averaged over ~2500 runs with single atoms. The shaded area represents the absence of 60 photons (per atom) from the transmitted field.

measure the transmission, we coupled a weak probe field into the waveguide by scattering a focused beam off of the free-standing tip of the waveguide and collected the transmitted light through the tapered optical fiber supporting the waveguide. With the atom placed at the cavity mode maximum (x = +0.8 μm) (Fig. 3D), we recorded the transmission of light near the $F = 2 \rightarrow F' = 3$ transition, as shown in Fig. 4. The atom decreases the cavity transmission by at most 2.2%, and the full-width at half-maximum (FWHM) of the transmission dip is ~26 MHz, which is four times larger than the natural linewidth. The reduction lasts for ~1 ms before the atom is lost from the trap, during which time it scatters ~60 photons. The lifetime of the atom in the absence of the probe field is 250 ms; the lifetime is shortened by heating from photon scattering when the probe field is present.

The line broadening results mainly from optical pumping of the atom to other magnetic sublevels with different optical transition frequencies (fig. S6). This occurs after scattering only a few photons because the cavity field is linearly polarized and does not drive a closed cycling transition. We have modeled the line broadening using numerical simulations of the master equation for a single Rb atom, including the 12 relevant Zeeman states of the $F = 2 \rightarrow F' = 3$ transition (*22*), and find reasonable agreement between the model, the data, and the predicted coupling strength. The model, shown by the red line in Fig. 4, yields an estimate of $\eta = 0.07(1)$ and cavity QED parameters of $(2g,\kappa,\Gamma) = (2\pi) \times [0.60(8), 840(80), 0.006]$ GHz for the $|2,0\rangle \rightarrow |3,0\rangle$ transition. This Rabi frequency $2g$ is in excellent agreement with estimates based on numerical models of the optical potential and cavity geometry, which yield a trap-surface distance of z_0 = 260 nm and $2g/(2\pi) \sim 620$ MHz on the $|2,0\rangle \rightarrow |3,0\rangle$ transition.

Several straightforward improvements can be made to increase the atom-photon coupling. An optimized waveguide geometry will allow $z_0 < 130$ nm, increasing $2g/(2\pi)$ to 3 GHz (*22*). Additionally, quality factors as high as $Q = 3 \times 10^5$ have already been demonstrated for silicon nitride PWCs (*26*), which is an improvement of over 600 from our present cavity. These two improvements together give a cooperativity of $\eta > 1000$. Even stronger coupling can potentially be accessed by trapping atoms inside the holes in the waveguide by using alternative PWC geometries to create the necessary trapping potentials (*25*).

The present technique opens up prospects for realizing a wide variety of hybrid quantum systems. For example, the method can be used to deterministically load multiple traps on the same or different PWCs, as well as cavities forming a two-dimensional network on a chip. In combination with the parallel fabrication and integration possible with nano-photonics, this represents a promising route toward realizing complex nano-optical circuits with several atomic qubits. Potential applications range from quantum nonlinear optics to quantum networks and novel many-body systems (*27*, *28*).

Furthermore, the demonstrated trapping technique can be applied to other systems in which it is beneficial to control atoms near surfaces, such as quantum interfaces between ultracold atoms and mechanical oscillators (*15*) or electromagnetic circuits on a chip (*29*). It can also be used for nanoscale sensing or to probe atom-surface interactions at sub-micrometer scales. By starting from a quantum-degenerate gas it may be possible to simultaneously load multiple near-field traps separated by distances considerably smaller than $\lambda/2$ (*30*, *31*). This will allow studies of strongly correlated states to be extended into a new regime of high atomic densities and strong, long-range interactions.

References and Notes

1. C. Monroe, M. Lukin, *Phys. World* **21**, 32 (2008).
2. M. Wallquist, K. Hammerer, P. Rabl, M. Lukin, P. Zoller, *Phys. Scr.* **T137**, 014001 (2009).
3. B. Dayan *et al.*, *Science* **319**, 1062 (2008).
4. M. Hijlkema *et al.*, *Nature* **3**, 253 (2007).
5. D. E. Chang, A. S. Sørensen, E. A. Demler, M. Lukin, *Nat. Phys.* **3**, 807 (2007).
6. K. Hennessy *et al.*, *Nature* **445**, 896 (2007).
7. I. Fushman *et al.*, *Science* **320**, 769 (2008).
8. H. J. Kimble, *Nature* **453**, 1023 (2008).
9. C. Nölleke *et al.*, *Phys. Rev. Lett.* **110**, 140403 (2013).
10. I. Dotsenko *et al.*, *Phys. Rev. Lett.* **95**, 033002 (2005).
11. R. Gehr *et al.*, *Phys. Rev. Lett.* **104**, 203602 (2010).
12. J. Beugnon *et al.*, *Nat. Phys.* **3**, 696 (2007).
13. W. S. Bakr, J. I. Gillen, A. Peng, S. Fölling, M. Greiner, *Nature* **462**, 74 (2009).
14. Y. Lin, I. Teper, C. Chin, *Phys. Rev. Lett.* **92**, 050404 (2004).
15. D. Hunger *et al.*, *Phys. Rev. Lett.* **104**, 143002 (2010).
16. E. Vetsch *et al.*, *Phys. Rev. Lett.* **104**, 203603 (2010).
17. A. Goban *et al.*, *Phys. Rev. Lett.* **109**, 033603 (2012).
18. N. Schlosser, G. Reymond, I. Protsenko, P. Grangier, *Nature* **411**, 1024 (2001).
19. R. A. Cornelussen, A. H. van Amerongen, B. T. Wolschrijn, R. Spreeuw, H. B. van Linden van den Heuvell, *Eur. Phys. J. D* **21**, 347 (2002).
20. D. E. Chang *et al.*, *Phys. Rev. Lett.* **103**, 123004 (2009).
21. J. D. Thompson, T. G. Tiecke, A. S. Zibrov, *Phys. Rev. Lett.* **110**, 133001 (2013).
22. Materials and methods are available as supplementary materials on *Science* Online.
23. J. S. Foresi *et al.*, *Nature* **390**, 143 (1997).
24. B. Lev, K. Srinivasan, P. Barclay, O. Painter, H. Mabuchi, *Nanotechnology* **15**, S556 (2004).
25. C. L. Hung, S. M. Meenehan, D. E. Chang, O. Painter, H. J. Kimble, Trapped atoms in one-dimensional photonic crystals; available at http://arxiv.org/abs/1301.5252 (2013).
26. M. Eichenfield, R. Camacho, J. Chan, K. J. Vahala, O. Painter, *Nature* **459**, 550 (2009).
27. M. J. Hartmann, F. G. S. L. Brandao, M. B. Plenio, *Nat. Phys.* **2**, 849 (2006).
28. A. D. Greentree, C. Tahan, J. H. Cole, L. C. L. Hollenberg, *Nature* **2**, 856 (2006).
29. A. André *et al.*, *Nat. Phys.* **2**, 636 (2006).
30. M. Gullans *et al.*, *Phys. Rev. Lett.* **109**, 235309 (2012).
31. O. Romero-Isart, C. Navau, A. Sanchez, P. Zoller, J. I. Cirac, Superconducting vortex lattices for ultracold atoms; available at http://arxiv.org/abs/1302.3504 (2013).

Acknowledgments: We acknowledge helpful discussions with O. Painter, D. Chang, M. Loncar, Q. Quan, E. Kuznetsova, S. Yelin, H. Park, and M. Greiner. Financial support was provided by the NSF, the Center for Ultracold Atoms, the Defense Advanced Research Projects Agency (QUASAR program), the Air Force Office of Scientific Research Multidisciplinary University Research Initiative, European Union project AQUTE, and the Packard Foundation. J.D.T. acknowledges support from the Fannie and John Hertz Foundation and the NSF Graduate Research Fellowship Program, N.P.d.L. acknowledges an Element Six postdoctoral fellowship, and J.F. acknowledges a grant from the NSF through ITAMP. This work was performed in part at the Center for Nanoscale Systems (CNS), a member of the National Nanotechnology Infrastructure Network, which is supported by NSF award ECS-0335765. CNS is part of Harvard University.

Supplementary Materials

www.sciencemag.org/cgi/content/full/science.1237125/DC1
Materials and Methods
Figs. S1 to S6
References (*32*–*38*)

26 February 2013; accepted 15 April 2013
Published online 25 April 2013;
10.1126/science.1237125

Entanglement Polytopes: Multiparticle Entanglement from Single-Particle Information

Michael Walter,[1]* Brent Doran,[2] David Gross,[3] Matthias Christandl[1]

Entangled many-body states are an essential resource for quantum computing and interferometry. Determining the type of entanglement present in a system usually requires access to an exponential number of parameters. We show that in the case of pure, multiparticle quantum states, features of the global entanglement can already be extracted from local information alone. This is achieved by associating any given class of entanglement with an entanglement polytope—a geometric object that characterizes the single-particle states compatible with that class. Our results, applicable to systems of arbitrary size and statistics, give rise to local witnesses for global pure-state entanglement and can be generalized to states affected by low levels of noise.

Entanglement is a uniquely quantum mechanical feature. It is responsible for fundamentally new effects, such as quantum nonlocality, and constitutes the basic resource for concrete tasks such as quantum computing (*1*) and interferometry beyond the standard limit